Remote Sens. **2012**, *4*, 3781-3795; doi:10.3390/rs4123781

OPEN ACCESS

Remote Sensing

ISSN 2072-4292

www.mdpi.com/journal/remotesensing

Article

Satellite-Derived Photic Depth on the Great Barrier Reef: Spatio-Temporal Patterns of Water Clarity

Scarla Weeks [1,*], P. Jeremy Werdell [2], Britta Schaffelke [3], Marites Canto [1], Zhongping Lee [4], John G. Wilding [2] and Gene C. Feldman [2]

[1] Biophysical Oceanography Group, School of Geography, Planning and Environmental Management, University of Queensland, Brisbane, QLD 4072, Australia; E-Mail: m.canto@uq.edu.au

[2] Ocean Biology Processing Group, Goddard Space Flight Center, NASA Greenbelt, MD 20771, USA; E-Mails: jeremy.werdell@nasa.gov (P.J.W.); john.g.wilding@nasa.gov (J.G.W.); gene.c.feldman@nasa.gov (G.C.F.)

[3] Australian Institute of Marine Science, PMB 3, Townville, QLD 4810, Australia; E-Mail: b.schaffelke@aims.gov.au

[4] Department of Environmental, Earth and Ocean Sciences, University of Massachusetts, Boston, MA 02125, USA; E-Mail: zhongping.lee@umb.edu

***** Author to whom correspondence should be addressed; E-Mail: s.weeks@uq.edu.au; Tel.: +61-7-3346-9056; Fax: +61-7-3365-6899.

Received: 8 October 2012; in revised form: 15 November 2012 / Accepted: 20 November 2012 / Published: 27 November 2012

Abstract: Detecting changes to the transparency of the water column is critical for understanding the responses of marine organisms, such as corals, to light availability. Long-term patterns in water transparency determine geographical and depth distributions, while acute reductions cause short-term stress, potentially mortality and may increase the organisms' vulnerability to other environmental stressors. Here, we investigated the optimal, operational algorithm for light attenuation through the water column across the scale of the Great Barrier Reef (GBR), Australia. We implemented and tested a quasi-analytical algorithm to determine the photic depth in GBR waters and matched regional Secchi depth (Z_{SD}) data to MODIS-Aqua (2002–2010) and SeaWiFS (1997–2010) satellite data. The results of the *in situ* Z_{SD}/satellite data matchup showed a simple bias offset between the *in situ* and satellite retrievals. Using a Type II linear regression of log-transformed satellite and *in situ* data, we estimated Z_{SD} and implemented the validated Z_{SD} algorithm to generate a decadal satellite time series (2002–2012) for the GBR. Water clarity varied significantly in space and time. Seasonal effects were distinct, with lower

values during the austral summer, most likely due to river runoff and increased vertical mixing, and a decline in water clarity between 2008–2012, reflecting a prevailing La Niña weather pattern. The decline in water clarity was most pronounced in the inshore area, where a significant decrease in mean inner shelf Z_{SD} of 2.1 m (from 8.3 m to 6.2 m) occurred over the decade. Empirical Orthogonal Function Analysis determined the dominance of Mode 1 (51.3%), with the greatest variation in water clarity along the mid-shelf, reflecting the strong influence of oceanic intrusions on the spatio-temporal patterns of water clarity. The newly developed photic depth product has many potential applications for the GBR from water quality monitoring to analyses of ecosystem responses to changes in water clarity.

Keywords: water clarity; photic depth; Secchi depth; satellite; Great Barrier Reef; spatio-temporal patterns; biophysical processes

1. Introduction

The quantification of environmental variables in space and time is essential to understand the ecology of marine organisms and their responses to a changing environment. For benthic organisms, temperature, salinity and the availability of light and nutrients are key parameters controlling their distribution and productivity. Ocean color satellites, such as the NASA Sea-viewing Wide Field-of-view Sensor (SeaWiFS) and the NASA Moderate Imaging Spectroradiometer onboard Aqua (MODIS-Aqua), provide oceanographic data records on spatial and temporal scales unattainable using conventional *in situ* sampling schemes. The current state of operational satellite remote sensing is that algorithms for measuring geophysical parameters, such as chlorophyll concentration or water clarity, are reasonably reliable over deep water, but still limited in optically shallow regions. Considerable progress has, however, been made in the application of polar orbiting satellite data to mapping nearshore optical properties [1–3]. Recent progress in remote sensing applications includes the development of bio-optical algorithms for determining the photic depth ($Z_{\%}$; units of m) from the observed satellite radiances. $Z_{\%}$ is a measure of water clarity [4] with, for example, $Z_{1\%}$ reflecting the depth where only 1% of the surface irradiance (PAR, photosynthetic available radiation; units of $\mu E\ cm^2\ s^{-1}$) remains. The value of 1% of surface PAR has been conveniently considered as an ecologically important threshold, the "euphotic depth", or lower limit of the euphotic zone, or "compensation depth", a depth below which most photo-autotrophic organisms cannot achieve positive net daily production [5,6]. The euphotic depth relates inversely to light attenuation and, thus, provides a direct, intuitive measure of the clarity or transparency of the overlying water column [5].

Detecting changes to the transparency of the water column is critical for understanding the responses of benthic organisms to light availability, especially in shallow coastal and shelf regions, such as the Great Barrier Reef (GBR), Australia [7,8]. Degradation in the condition of coastal and inshore ecosystems due to poor water quality is a key issue for the GBR [9], as terrestrial runoff of excess nutrients and sediments affects turbidity and sedimentation regimes and intermittently increases water column productivity, in turn leading to the deterioration of inshore coral reefs at local scales [10].

Water clarity is considered a key measure of water quality on the GBR, with Secchi depth (Z_{SD}; units of m) being the most widely used measure. Measurements of optical properties of the water are usually carried out during dedicated bio-optical research cruises and, therefore, are limited in number, while Z_{SD} is a common and easily obtained parameter in monitoring, making it suitable for satellite data evaluation [11]. A water quality trigger level of Z_{SD} < 10 m has been formulated for the GBR [12], below which macroalgal cover rapidly increases and coral richness declines [8]. However, the links between reef health and water quality at GBR-wide scales remain the subject of debate due to the limited availability of large-scale data. For large ecosystems, such as the GBR, efficient ocean-color algorithms that can produce accurate synoptic satellite imagery and estimates of water-column optical properties, such as water clarity, are essential for understanding the links between oceanographic processes and the biological response.

The circulation in the GBR region is complex, with variability in the physical processes significantly influencing the patterns of water clarity. The GBR ecosystem extends along the continental shelf of northeastern Australia between 9 °S and 24 °S and covers ~345,000 km^2, including approximately 2,900 coral reefs. The direction of water currents on the inner GBR shelf is primarily northward, driven by the predominant southeast wind regime. Along the outer shelf, the South Equatorial Current bifurcates to form the northward-flowing Hiri Current and the southward-flowing East Australian Current (EAC) [13]. The location of the bifurcation varies seasonally between 14 °S, during austral summer, when the EAC is strongest, and 20 °S during austral winter. Drifter studies have suggested another bifurcation at around 19 °S, and within the GBR lagoon, a strong and consistent northwest flow north of 18 °S and a weaker and more variable flow south of 18 °S, with limited water exchange between the two latitudinal regions [14]. In the southern GBR, the deep (80–150 m) Capricorn Channel separates the inner and the outer shelf into two distinct reef systems, while a stable cyclonic eddy, the Capricorn Eddy, typically forms in the lee of the shelf bathymetry [15]. Estimates of water residence times for the GBR lagoon differ between recent studies, ranging from weeks [14,16,17] to several months [13,18]. Analyses of satellite imagery of riverine flood plumes suggest water residence times of several weeks in the coastal and inshore GBR [19,20].

The primary objectives of this study were: (1) to develop a photic depth product for the GBR; (2) to detect changes in GBR water clarity in space and time based on the optimal, available algorithm for light attenuation through the water column; and (3) to determine the dominant modes of variation and identify the physical drivers that influence the spatio-temporal patterns of water clarity across the GBR ecosystem.

2. Data and Methods

Since sufficient GBR *in situ* optical data were not readily available for validation purposes, regional measurements of Z_{SD} collected by the Australian Institute of Marine Science (AIMS) and the Queensland Department of Primary Industries and Fisheries (QDPI) were used to serve as a first order ground-truth for the satellite data products, with over 5,000 records acquired. These data were somewhat biased towards the inshore region (Figure 1), due to the focus of the regional research and monitoring programs, with Z_{SD} often quite low (<5 m). Such values are not unusual in GBR inshore waters, which experience intermittent high turbidity due to resuspension and flood inputs. Higher Z_{SD}

values were generally found further offshore. The timeframes of the data (1994–1999; 1992–2010) largely pre-dated the MODIS-Aqua satellite data (2002–2010), hence SeaWiFS data (1997–2010) were also used to validate and improve the photic depth product for the GBR ecosystem.

Figure 1. Map of Secchi depth measurement locations (red) in the Great Barrier Reef from 1994 to 2010.

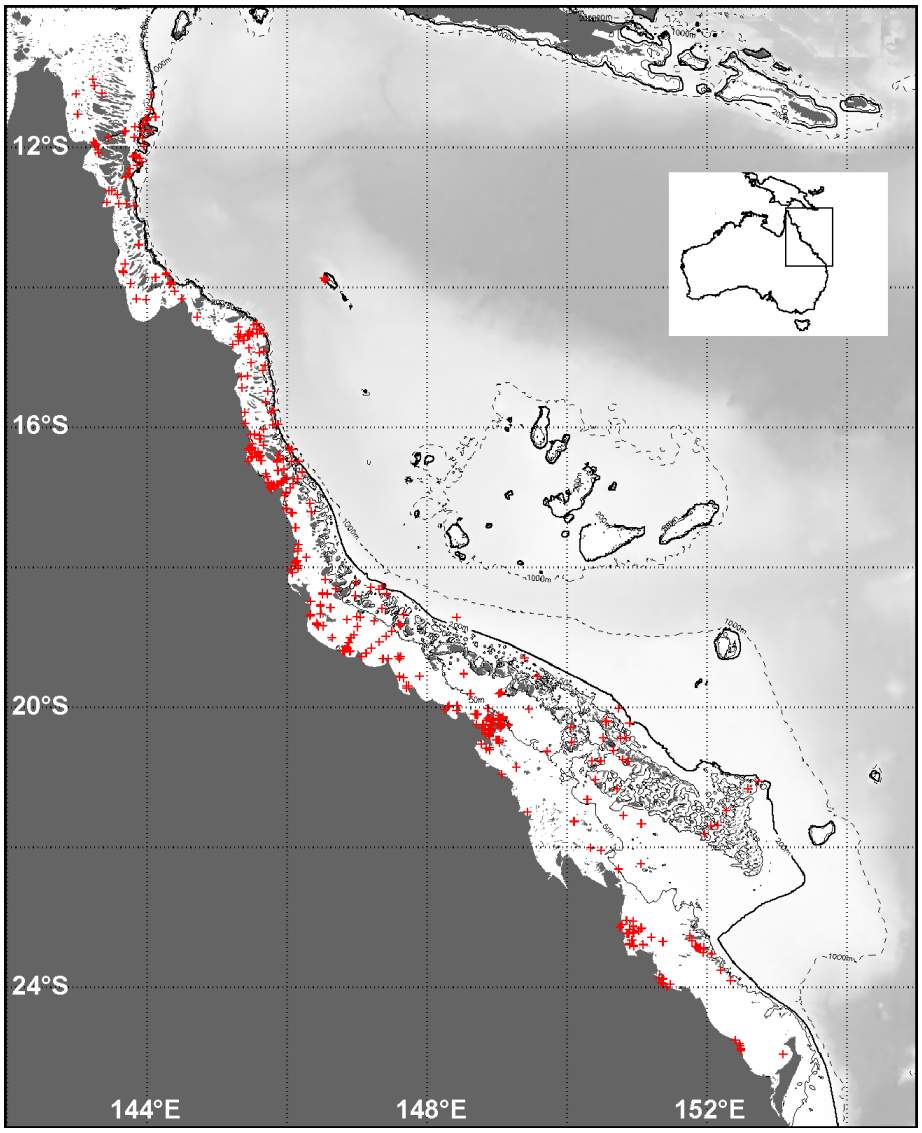

Two operational photic depth algorithms have been implemented into the standard NASA ocean color satellite data processing environment, both of which are available via the SeaWiFS Data Analysis System (SeaDAS; http://oceancolor.gsfc.nasa.gov/seadas): an empirical algorithm based on Case-1 assumptions [21] and a semi-analytical algorithm based on the inherent optical properties (IOPs) of the water column [4]. The IOP approach, where photic depth is described as a function of spectral absorption and backscattering coefficients, was selected for this study as the water-clarity algorithm to determine light penetration depth in eutrophic, Case-2 coastal waters [6]. This algorithm has been tested and validated for oceanic and coastal waters in the Arabian Sea, Monterey Bay, Gulf of Mexico and Yellow Sea [4], but not in the GBR.

In this study, IOPs from the quasi-analytical algorithm (QAA; [2]) were used to determine the depth where 10% of the surface light (PAR) level was still available, $Z_{10\%}$, which was in turn regionally tuned to Z_{SD} using "matchups" with *in situ* Z_{SD} data. The satellite-to-*in situ* matchups for the AIMS and QDPI *in situ* Z_{SD} dataset were acquired from the NASA Ocean Biology Processing Group (OBPG) [22]. Matchups were generated for both SeaWiFS and MODIS-Aqua. These matchups were generated using the methods and quality assurance procedures described in Bailey and Werdell [23], which included: (1) locating satellite observations made within ± 3-hours of the time of *in situ* data collection; (2) calculating the filtered median of all unflagged pixels within a 5 × 5 pixel box centered on the *in situ* target; and (3) excluding any matchups where the coefficient-of-variation of the unflagged satellite pixels exceeded 0.15. To the best of our knowledge, we excluded matchup stations in optically shallow water, where light reflected off of the sea floor contributes to the water-leaving signal observed by the satellite.

A regression of the *in situ* Z_{SD} values against the matching satellite estimates of $Z_{10\%}$ was used to adjust the satellite-derived $Z_{10\%}$ to Z_{SD}. A Type II linear regression (RMA) of log-transformed satellite and *in situ* data was used to estimate Z_{SD} for the GBR according to:

$$Z_{SD} = 10\text{^}[\{\log_{10}(Z_{10\%}) - a_0\}/a_1] \quad (1)$$

where a_0 and a_1 are 0.518 and 0.811 for SeaWiFS (N = 235; r^2 = 0.78; RMSE = 0.148) and 0.529 and 0.816 for MODIS-Aqua (N = 71; r^2 = 0.83; RMSE = 0.096). This method for regional tuning is ultimately insensitive to our choice of a specific $Z_{\%}$, as the assignment of percent light level in Lee *et al.* [4] changes only the absolute magnitude of the depth estimates, not their variability. For example, had we used $Z_{37\%}$ in Equation (1), a_0 and a_1 would be different than reported above, but their derived Z_{SD} would not. Finally, this GBR-validated Z_{SD} algorithm was implemented into the SeaDAS environment and applied to the full regional time series of MODIS-Aqua data (2002–2012). Daily, monthly and decadal means and anomalies were generated at 1-km^2 resolution and analyses undertaken. For the purpose of this study, the analyses focused on the central to southern GBR (S-GBR, 18 °S–24 °S).

To represent the temporal evolution of water clarity on the S-GBR over the last decade (July 2002 to June 2012), latitude-time Hovmöller diagrams were generated for both the S-GBR continental shelf and inshore lagoon regions. Bathymetry masks were created to limit the spatial domains to 0–200 m and 0–35 m for the shelf and inshore regions, respectively, excluding topographic reef features. Monthly mean Z_{SD} values were averaged along each ~0.01 ° line of latitude (1-km resolution) for each of the selected masked areas. Pixels coinciding with missing values (<3%) and over topographic reef features were ignored in the computation.

To characterize the variability of the satellite-derived Z_{SD} on the S-GBR, an Empirical Orthogonal Function (EOF) Analysis was performed on the ten-year monthly Z_{SD} dataset. An EOF Analysis is a statistical technique used to decompose the spatial and temporal variability of time series datasets into a few independent dominant modes, each representing a certain percentage of the total variance of the dataset. In this study, we employed the singular value decomposition (SVD) method [24] to calculate the spatial eigenfunctions and temporal eigenvectors. The former describes the spatial pattern associated with the mode, while the latter provides the corresponding temporal variation, which can be interpreted in relation to physical processes. The EOF assumes that there is no gap in the data time series. Hence, prior to doing the analysis, missing data over small gaps (<3% in total) were filled for

each monthly dataset, using a kernel interpolation [25]. The bathymetry mask was used to limit the spatial domain to the shelf area (0–200 m). The long-term (10 years) temporal mean was removed from the time series at each pixel location prior to analysis to reduce the dominant seasonal signal [24].

3. Results and Discussion

The results of the satellite-to-*in situ* "matchups" for the AIMS/QDPI Z_{SD} dataset were far better than expected, given that there had been no regional refinement of the IOP photic depth algorithm. The results showed primarily a simple bias offset between the *in situ* and satellite retrievals, with similar slopes and intercepts for SeaWiFS and MODIS-Aqua (Equation (1)). Using a linear regression of log-transformed data to generate the GBR-validated Z_{SD} algorithm eliminated negative values returned for Z_{SD} when the regression was applied in normal space. Figure 2 shows the MODIS-Aqua GBR satellite-to-*in situ* matchups tuned using log-transformed data in the regression.

Figure 2. MODIS-Aqua GBR satellite-to-*in situ* matchups using the GBR-validated algorithm. Panel (**a**) shows *in situ* Z_{SD} *versus* MODIS-Aqua $Z_{10\%}$ with the best fit (Equation (1)) shown in red. Panels (**b**) and (**c**) compare *in situ* Z_{SD} with MODIS-Aqua Z_{SD} from the GBR-validated algorithm. A Type II linear regression analysis of the results presented in (b) yields N = 71, r^2 = 0.63, RMSE = 3.45 and slope = 1.03, and intercept =−0.25).

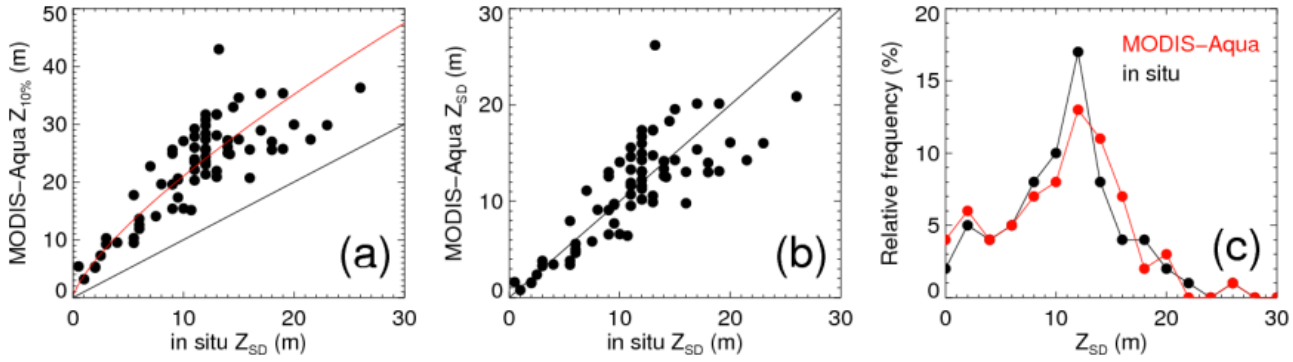

The GBR-validated Z_{SD} time series of monthly and decadal means generated from MODIS-Aqua data showed considerable seasonality in water clarity, with distinct patterns of spatial distribution. On the GBR shelf, inshore waters were generally more turbid than further offshore, with waters most turbid during March and most transparent during September (Figure 3). This distinct seasonal variation is due to variability in the ocean-atmosphere dynamics, with more turbid waters in the austral summer (Figure 3(a)), the "wet season" on the GBR, when the prevailing north-westerlies and the Coriolis effect result in primarily offshore surface flow of sediment-laden waters from river discharge and increased vertical mixing. During austral winter, or the "dry season" on the GBR, the prevailing southeasterly trade winds dominate, limiting cross-shelf surface flow. Furthermore, seasonal strengthening of the southward-flowing EAC in early spring (September–October), when the opposing trade winds begin to subside [26–28], results in strong intrusions of clear, oligotrophic EAC waters through the Palm and Magnetic Passages in the central GBR [29], with southward flow along the mid-shelf channel (Figure 3(b)). At the southern end of the GBR, the Capricorn Eddy forms most

strongly during spring when the EAC strengthens, with resultant intrusions of clear EAC waters into the Capricorn and Curtis Channels [15], further enhancing separation of the inner and outer shelf regions (Figure 3(b)).

Figure 3. Long-term (2002–2012) monthly mean Secchi depth (m) on the central-southern Great Barrier Reef showing waters most turbid (**a**) during March and most transparent (**b**) during September. The solid black line denotes the 200 m isobath. The large white arrow represents the southward flow of the East Australian Current, with smaller white arrows showing the directions of oceanic intrusions onto the shelf. The circular arrows show the location of the Capricorn Eddy (E) that forms in the lee of the shelf bathymetry.

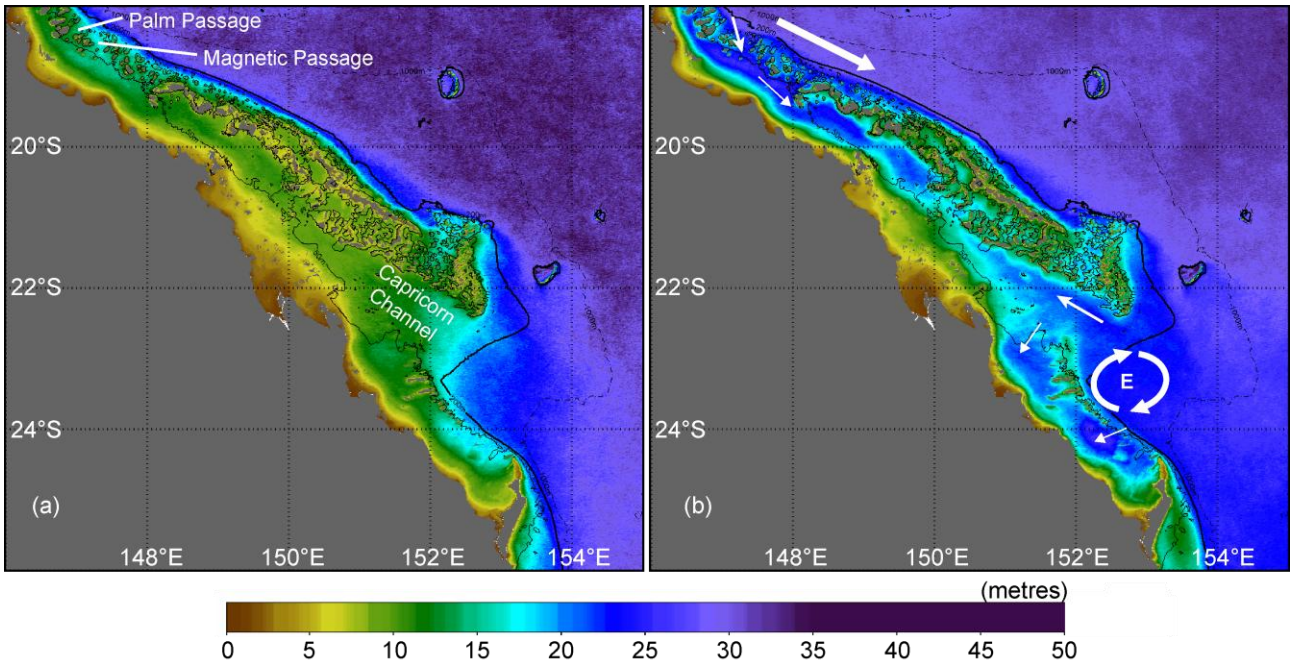

The Z_{SD} anomalies clearly showed areas and times where water clarity was anomalously poor, following periods of increased cyclonic or storm activity. For example, intense positive anomalies followed excessive storm activity in March 2009, with the cross-shelf extent and turbid water track of Tropical Cyclone (TC) Hamish, a powerful category 5 storm, clearly visible along the continental shelf edge of the S-GBR, even extending offshore as far as the 1,000 m isobath (Figure 4(a)). Similarly, the newly implemented GBR Z_{SD} product allowed near-realtime tracking of the intrusion of anomalous conditions following TC Yasi (category 5) that impacted the central GBR in February 2011 (Figure 4(b)). In contrast, the strongest negative anomalies occurred in September 2008 (Figure 4(c)), when intrusions of clear oceanic waters appeared particularly intense, both into the central GBR channel and from the south, into the Capricorn and Curtis Channels.

The Hovmöller diagrams illustrate the variation of water clarity on the S-GBR in space (latitude) and time (July 2002 to June 2012), both across the entire continental shelf (Figure 5) and along the inshore region (Figure 6). A distinct seasonal signal is apparent on the S-GBR shelf (Figure 5), with water generally more turbid in late summer (February to April) and clearest in late winter/early spring (August to October). Spatially, mean water clarity across the shelf is higher in latitudinal bands coincident with intrusions of oceanic waters in the central (between 18.25 °S and 19.25 °S) and

southern GBR (between 22.25 °S and 23.25 °S). However, most notable is the decline in water clarity in recent years, with a significant decrease in mean shelf Z_{SD} of 2.00 m (from 13.9 m to 11.9 m) over the last decade, after removal of the seasonal signal ($F = 10.58$; $p < 0.0015$; $n = 120$). A progressive increase in space-time for which the average cross-shelf Z_{SD} values remained below the critical water quality level for the GBR of <10 m Z_{SD} [8] is also apparent. Poor water clarity was especially pronounced in April to May 2012 (Figure 5), when mean cross-shelf Z_{SD} values of <8 m were experienced in the S-GBR, declining at locations to as low as 6 m in May, likely due to strong vertical mixing and intrusions onto the shelf of anomalously turbid waters following sustained, strong winds in the greater study region (Australian Bureau of Meteorology, http://www.bom.gov.au/).

Figure 4. Secchi depth anomalies (m) on the central-southern Great Barrier Reef (panel orientations rotated by 40 °). The dark and light black lines denote the 200 m and 1,000 m isobaths, respectively. Panel (**a**) shows intense positive anomalies and the turbid water track of Tropical Cyclone (TC) Hamish along the shelf edge from 14 to 17 March 2009. Panel (**b**) shows intrusions of turbid waters on 4–6 February 2011 following TC Yasi; and panel (**c**) shows strong negative anomalies from 12 to 17 September 2008 following intrusions of clear oceanic waters onto the shelf.

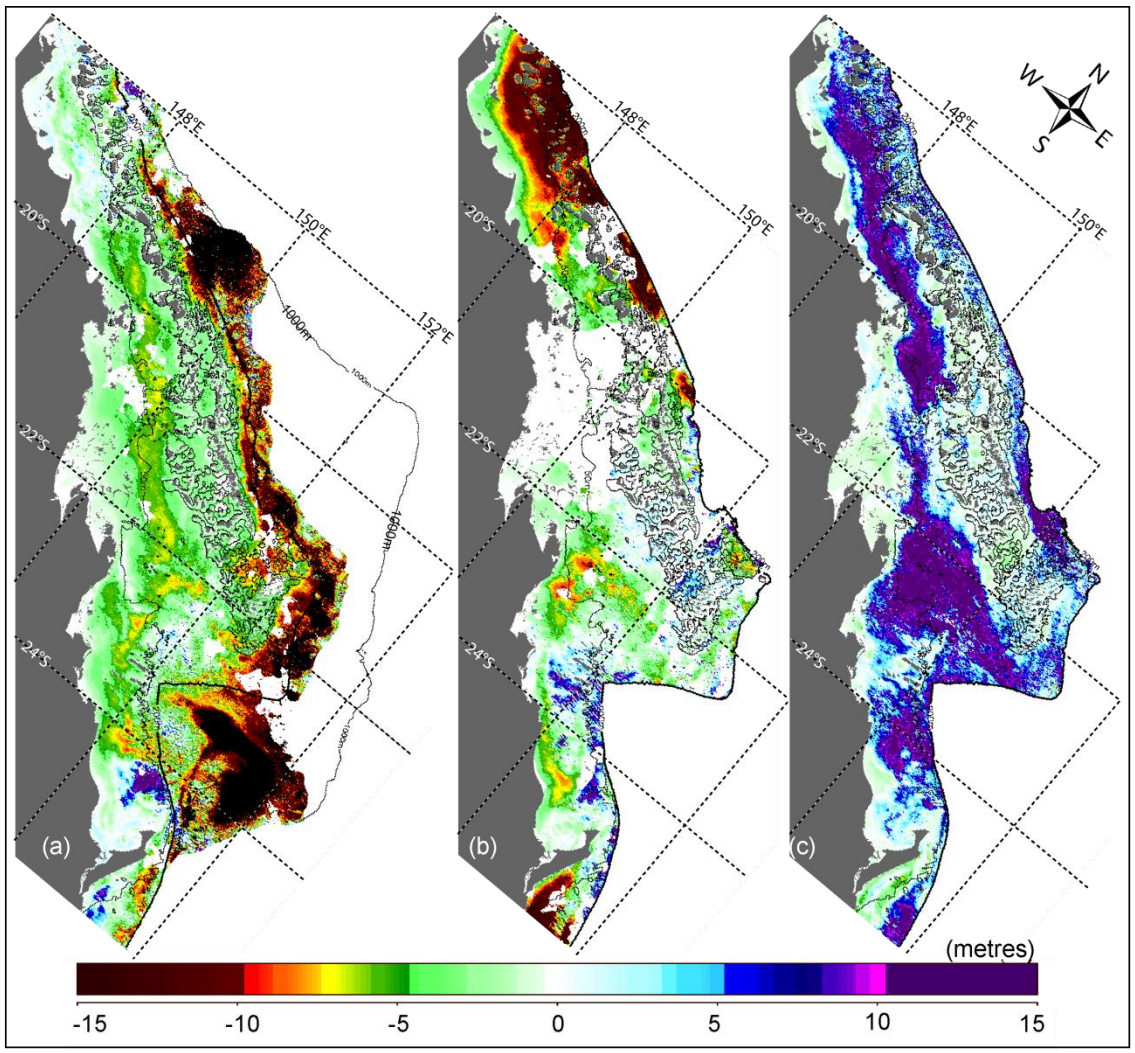

Figure 5. Hovmöller diagram illustrating the variation of water clarity on the central-southern Great Barrier Reef in space (18 °S–24 °S) and time (July 2002–June 2012). Areas with mean cross-shelf Secchi depth <10 m are highlighted by grey contour. The right-hand panel shows the bathymetry mask used to limit the spatial domain to 0–200 m, excluding reef features.

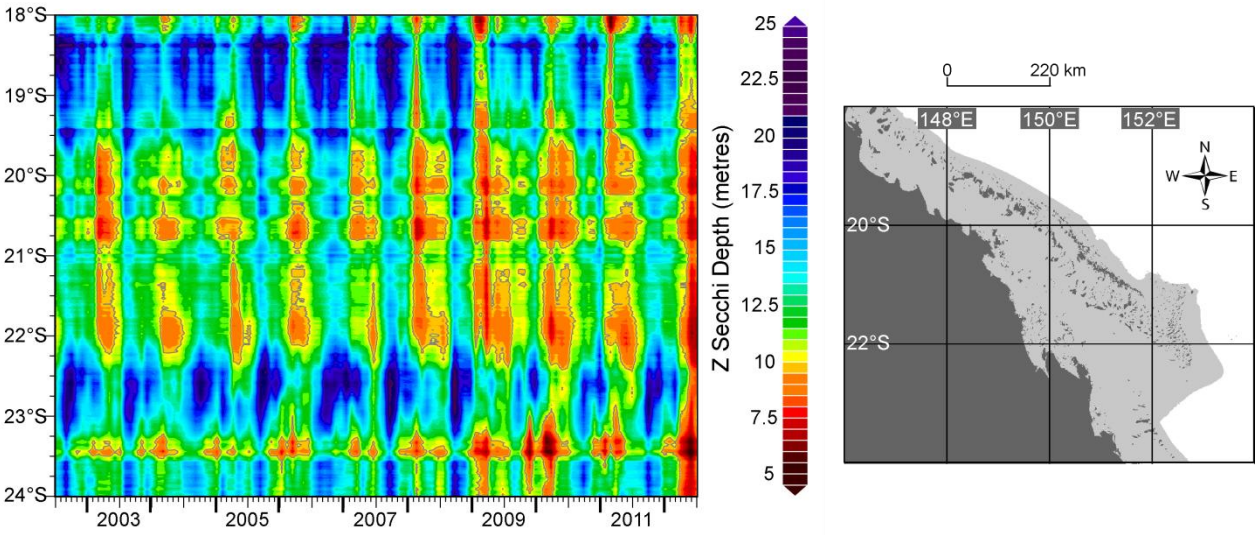

Figure 6. Hovmöller diagram illustrating the variation of water clarity on the inner shelf of the central-southern Great Barrier Reef in space (18 °S–24 °S) and time (July 2002–June 2012). Areas with mean Secchi depth <5 m are highlighted by grey contour. (**Right**) panel shows the bathymetry mask used to limit the spatial domain to 0–35 m, excluding reef features. The locations of (A) the Burdekin River, (B) Broad Sound, and (C) the Fitzroy River are annotated (**Left**).

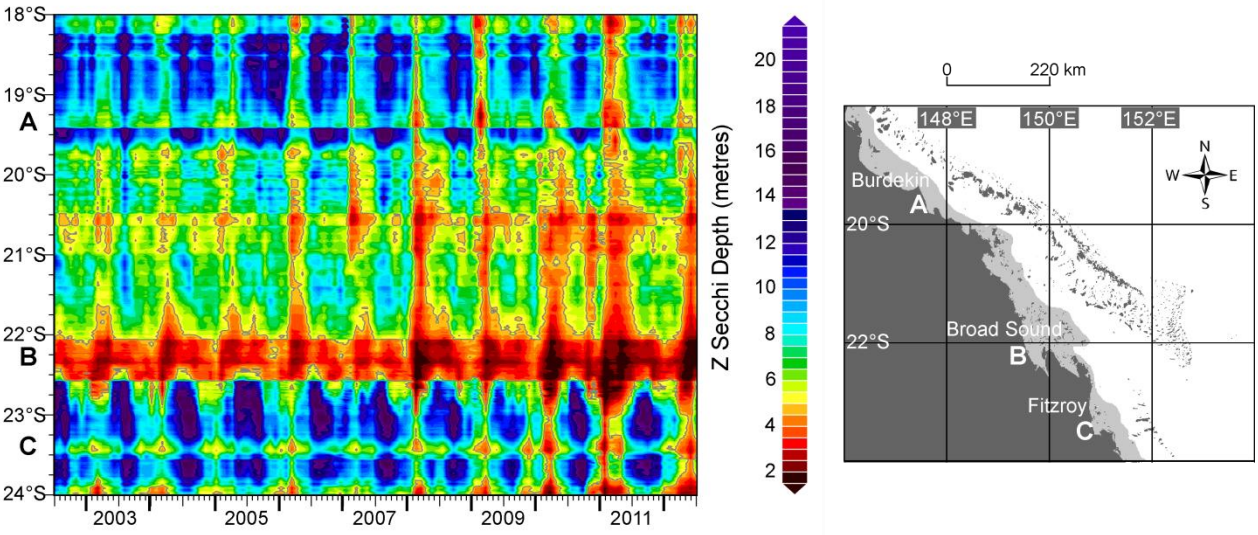

On the inner shelf (0–35 m), a distinct seasonal signal is also apparent (Figure 6), along with the turbid water signatures of the seasonal riverine inputs from the Burdekin (~19.4 °S) and Fitzroy Rivers (~23.5 °S), the two largest rivers in Queensland, which had above-median flows for the Burdekin from 2007–2012 and above-median flows for the Fitzroy in 2008 and 2010–2012, respectively. Also clearly

visible is Broad Sound (~22.1°S–22.4°S), an embayment where high tidal energy causes strong vertical mixing of the shallow waters, leading to low water clarity all-year-round. The decline in water clarity in recent years is even more pronounced in this inshore area where a significant decrease in mean inner shelf Z_{SD} of 2.1 m (from 8.3 m to 6.2 m) occurred over the last decade, after removal of the seasonal signal ($F = 10.58$; $p < 0.0015$; $n = 120$). From summer 2007/08 onwards, the areas and time periods markedly increased where Z_{SD} values remained below 5 m (Figure 6), which is half of the Z_{SD} trigger level for GBR waters [8,12]. These negative trends in water clarity coincided with the five years during which the GBR experienced strong La Niña conditions in 2007/08, 2008/09, 2010/11 and 2011/12 (Australian Bureau of Meteorology). In northeastern Australia, La Niña events are typically associated with an earlier onset of and a more vigorous summer monsoon, characterized by enhanced tropical cyclone activity and wetter summers [30–33]. The associated increased river discharge and vertical mixing is likely to be the main reason for the measured decrease in water clarity, especially of the shallow inner shelf waters.

The EOF Analysis decomposed the spatial and temporal variability of the Z_{SD} time series on the S-GBR shelf over the last decade into a few independent dominant modes, each representing a certain percentage of the total variance of the dataset. Only the first two dominant modes are presented here, explaining 51.3% and 10.7% of the total variance, respectively. Mode 1 (Figure 7), which accounts for over half of the total variance of the dataset, indicates a strong seasonal signal in photic depth variability on the S-GBR, with considerable interannual variation. The spatial pattern (Figure 7(a), normalized from −1.0 to +1.0) shows a consistent phase (positive in Figure 7(a)) across the entire shelf, with the most positive values (purple) in the mid-shelf region. The temporal eigenvectors for Mode 1 (Figure 7(b)) provide the temporal variation associated with the spatial pattern (Figure 7(a)) over the 10-year period. More positive eigenvalues indicate months when the shelf waters were clearer, whereas more negative eigenvalues represent months when water clarity was poorer. The greatest variance explained by Mode 1 occurred at locations where values are most positive in the spatial map (Figure 7(a)), with the clearest waters here during months when the eigenvalues (Figure 7(b)) were most positive, or conversely, the most turbid waters here during months when the eigenvalues were most negative. A pronounced pattern is apparent in the temporal variation, with more turbid waters in the first half of the year, generally from March to May, and clearer waters in the latter half, generally in September and October. Interannual variation is apparent across the time series with a change to reduced water clarity in more recent years.

However, most notable in Figure 7 is that the greatest variation in water clarity occurred along the mid-shelf, not in the inshore region directly exposed to seasonal river outflow, inferring a strong influence of oceanic intrusions during certain months. The combined spatial and temporal patterns show the clearest waters intruding through the Palm and Magnetic Passages and along the mid-shelf channel, and similarly, in the Capricorn Channel in the south. Furthermore, water clarity is generally greatest during early spring (Figure 7(b)), when the EAC strengthens and the southeast trade winds relax. This springtime acceleration of the EAC is known to lead to intrusions in the central GBR [27,29] and further to the south, the Capricorn Eddy forms most strongly and regularly in spring, with associated intrusions up the Capricorn Channel [15,28]. These intrusions onto the mid-shelf would somewhat separate the water bodies of the inner-shelf from the outer shelf waters. During the early months of the year, when the GBR is under the influence of the summer monsoon and associated increased river

outflows, northwesterly winds dominate, enhancing cross-shelf flow of more sediment-laden waters. The influence of the strong La Niña conditions experienced over the recent five years is apparent in the interannual variation (Figure 7(b)), where enhanced tropical cyclone activity, wetter summers, stronger northwesterlies and increased vertical mixing have impacted the entire shelf waters for many consecutive months. The dominance of Mode 1 (51.3%) further reinforces the strong influence of the varying physical dynamics on the spatio-temporal patterns of water clarity on the S-GBR.

Figure 7. Mode 1 of the Empirical Orthogonal Function Analysis explaining 51.3% of the total variance of water clarity on the central-southern Great Barrier Reef from July 2002 to June 2012. The spatial pattern (panel (**a**), normalized from −1.0 to +1.0) shows a positive phase across the entire shelf with the most positive values (purple) in the mid-shelf region. Panel (**b**) provides the temporal variation associated with the spatial pattern over the 10-year period.

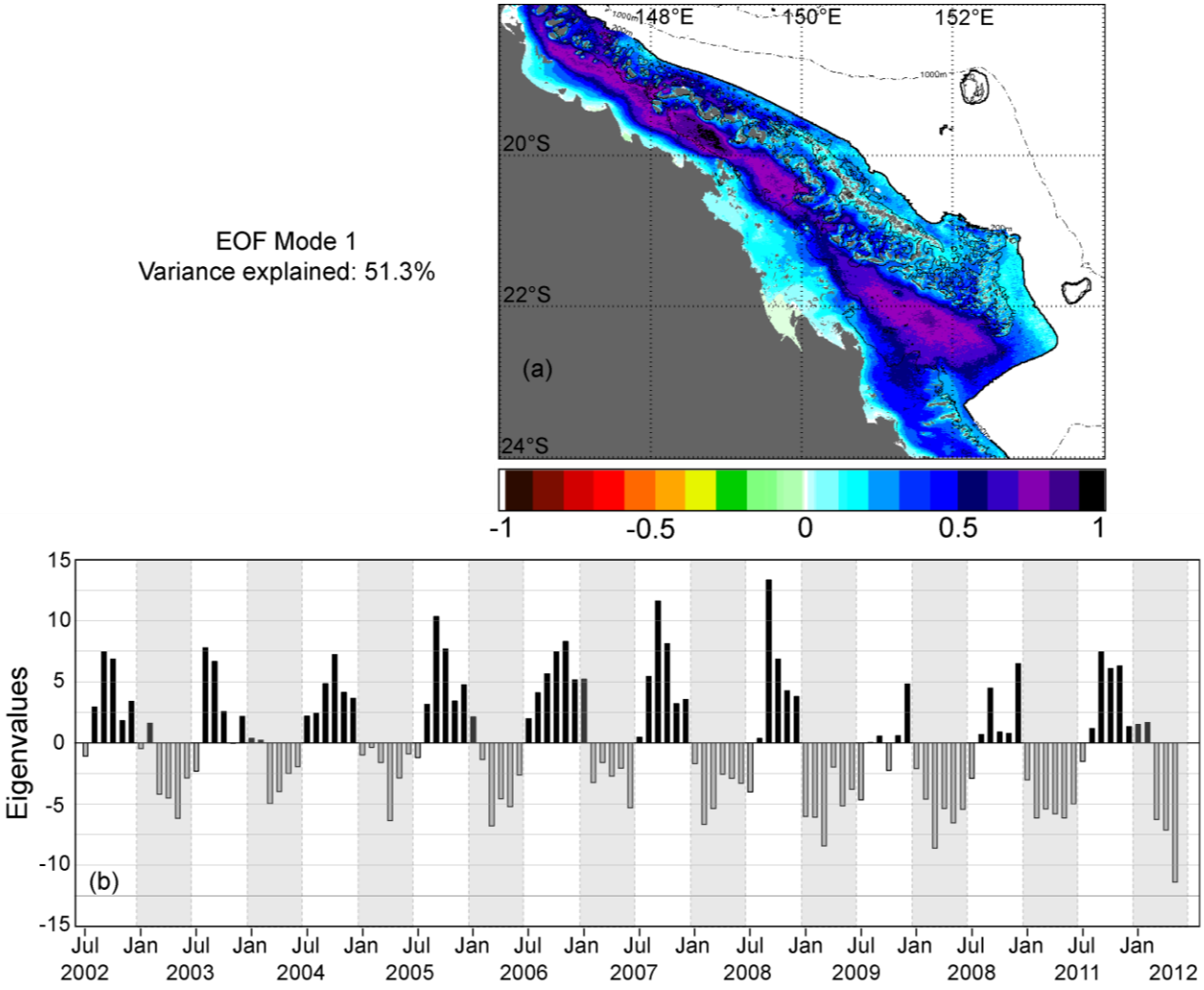

Mode 2 of the EOF Analysis (Figure 8) explains 10.7% of the total variance of Z_{SD} on the S-GBR shelf over the last decade. The spatial pattern (Figure 8(a), normalized from −1.0 to +1.0) shows generally positive values inshore and along the outer reefs, contrasting with negative values along the shelf edge, the mid-shelf and in the south. The associated temporal eigenvectors for Mode 2 (Figure 8(b)) show generally positive eigenvalues in autumn and winter, the "dry season" on the GBR, with negative

eigenvalues in spring and summer during the "wet season". Hence, during spring/summer for example, the negative eigenvalues combined with positive loadings in the spatial map show areas of poor water clarity and, where combined with negative spatial loadings, show areas of increased water clarity during those same months.

Figure 8. Mode 2 of the Empirical Orthogonal Function Analysis explaining 10.7% of the total variance of water clarity on the central-southern Great Barrier Reef (GBR) from July 2002 to June 2012. The spatial pattern (panel (**a**), normalized from −1.0 to +1.0) shows strong positive values intruding on the central GBR, and opposing positive/negative values in the south, relating most turbid waters coincident with strong East Australia Current dynamics. Panel (**b**) provides the temporal variation associated with the spatial pattern over the 10-year period.

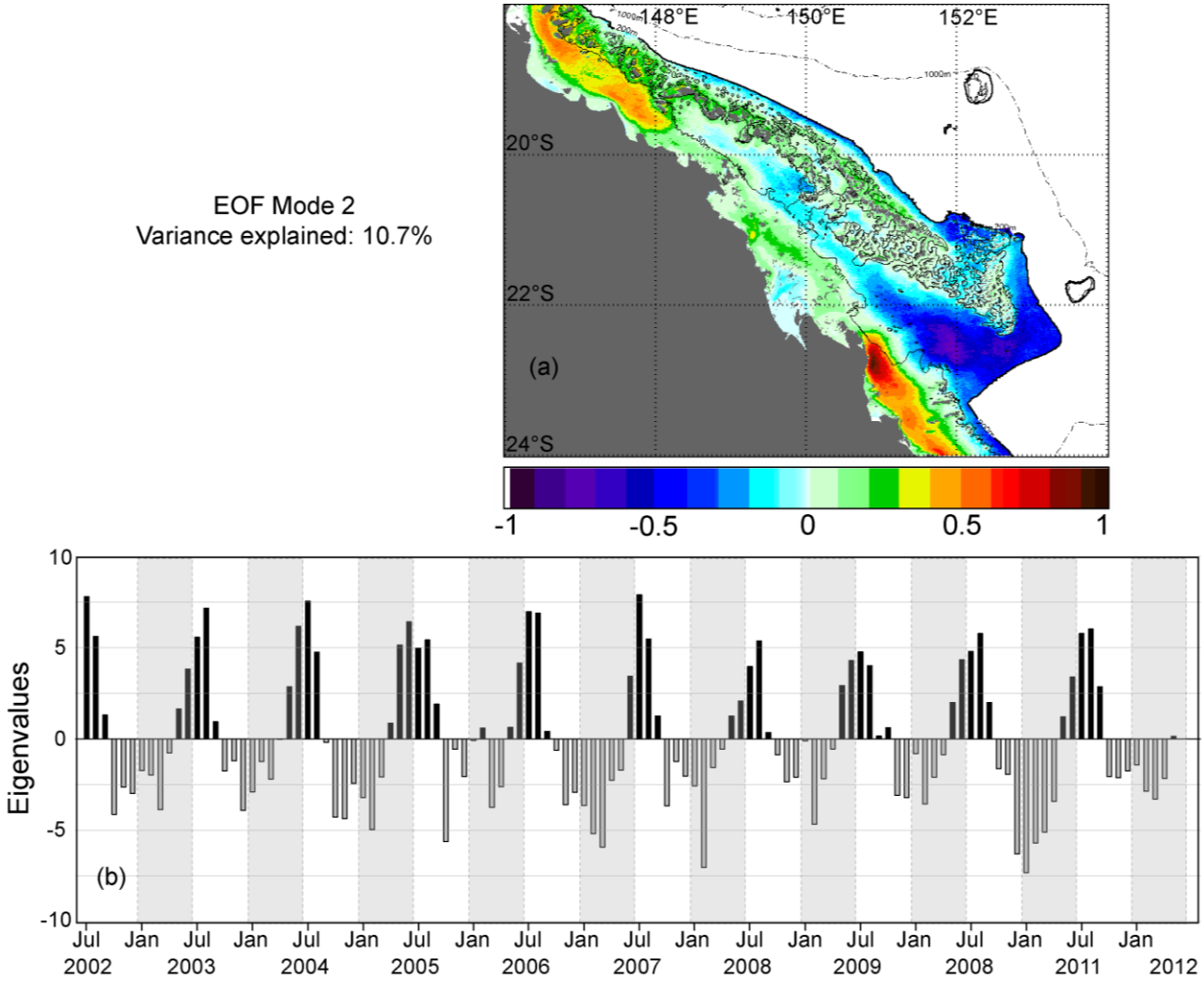

In the central GBR, the greatest variance appeared on the mid-shelf, primarily due to increased vertical mixing and intrusions onto the shelf of more turbid waters during summer, such as occurred when TC Yasi approached the central GBR in January 2011, as opposed to clearer waters in this area during winter. However, the greatest variance explained by Mode 2 occurred in the south, largely representing the offshore and spatial extent of river outflow. Here, the opposing positive/negative values in the spatial map show that the most turbid waters coincided with a strong EAC in summer

when clear oceanic waters flowed along the shelf-edge, skirted the Swains reefs in the south and intruded up the Capricorn Channel, containing any large river outflow inshore. This is especially notable in the long wet summer of 2010/11, when southeast Queensland experienced extreme flooding. The 2010–2011 wet season was characterized by extreme events in the GBR region, driven by a very strong La Niña, with the intense and prolonged rainfall resulting in the Fitzroy River having its largest flow in the instrumental record (approximately 38 million ML) [34]. However, of interest is that while the variance explained by Mode 2 appears related to storms and cyclonic events in summer, and consequent increased river discharge, variability in water clarity in the S-GBR was generally not most pronounced directly inshore where Z_{SD} remained persistently low.

4. Concluding Remarks

The Z_{SD} product generated from the implementation of the GBR-validated Z_{SD} algorithm allowed us to produce a long-term time series of water clarity data since 2002. Potential future applications of these data are, e.g., (i) to define baseline ranges of water clarity along and across the GBR to identify and quantify future changes in water clarity as a result of land use practice changes or other environmental changes such as climate change; and (ii) to analyze spatial and temporal patterns of change in reef communities in response to changes in water clarity.

Acknowledgments

We thank the NASA Ocean Biology Processing Group for assistance with the large volume of data processing and the development of the web-based validation search/display utility. Special thanks to B. Franz, S. Bailey, and C. Proctor for implementation of the Secchi depth algorithm into the SeaDAS environment and also to Bruce Monger for kindly providing his EOF code. The Australian Institute of Marine Science (www.aims.gov.au) and the Queensland Department of Primary Industries and Fisheries (now Queensland Department of Agriculture, Fisheries and Forestry, www.daff.qld.gov.au) are gratefully acknowledged for provision of *in situ* Secchi depth data. This research was funded by the Australian Research Council (Project LP100100342) and the Great Barrier Reef Foundation. Z.P. Lee was partially supported by the NASA Energy and Water Cycle Program (#NNX09AV97G).

References

1. Lee, Z. *Remote Sensing of Inherent Optical Properties: Fundamentals, Tests of Algorithms, and Applications*; Report of an IOCCG Working Group on Ocean-Colour Algorithms; International Ocean-Colour Coordinating Group: Dartmouth, NS, Canada, 2006.
2. Lee, Z.; Carder, K.L.; Arnone, R.A. Deriving inherent optical properties from water color: A multiband quasi-analytical algorithm for optically deep waters. *Appl. Opt.* **2002**, *41*, 5755–5772.
3. Qin, Y.; Brando, V.E.; Dekker, A.G.; Blondeau-Patissier, D. Validity of SeaDAS water constituents retrieval algorithms in Australian tropical coastal waters. *Geophys. Res. Lett.* **2007**, *34*, L21603.

4. Lee, Z.P.; Weidemann, A.; Kindle, J.; Arnone, R.; Carder, K.L.; Davis, C. Euphotic zone depth: Its derivation and implication to ocean-color remote sensing. *J. Geophys. Res.* **2007**, doi:10.1029/2006JC003802.
5. Falkowski, P.G.; Raven, J.A. *Aquatic Photosynthesis*; Blackwell Science: Malden, MA, USA, 1997; p. 375.
6. Kirk, J.T.O. *Light and Photosynthesis in Aquatic Ecosystems*, 2nd ed.; Cambridge University Press: Cambridge, UK, 1994; p. 509.
7. Fabricius, K.E.; De'ath, G.; Humphrey, C.; Zagorskis, I.; Schaffelke, B. Intra-annual variation in turbidity in response to terrestrial runoff on near-shore coral reefs of the Great Barrier Reef. *Estuar. Coast. Shelf Sci*. **2012**, doi:10.1016/j.ecss.2012.03.010.
8. De'ath, G.; Fabricius, K. Water quality as a regional driver of coral biodiversity and macroalgae on the Great Barrier Reef. *Ecol. Appl.* **2010**, *20*, 840–850.
9. Brodie, J.E.; Kroon, F.J.; Schaffelke, B.; Wolanski, E.C.; Lewis, S.E.; Devlin, M.J.; Bohnet, I.C.; Bainbridge, Z.T.; Waterhouse, J.; Davis, A.M. Terrestrial pollutant runoff to the Great Barrier Reef: An update of issues, priorities and management responses. *Mar. Pollut. Bull.* **2012**, *65*, 81–100.
10. Fabricius, K.E. Effects of terrestrial runoff on the ecology of corals and coral reefs: Review and synthesis. *Mar. Pollut. Bull.* **2005**, *50*, 125–146.
11. Kratzer, S.; Hakansson, B.; Sahlin, C. Assessing secchi and photic zone depth in the Baltic Sea from satellite data. *AMBIO* **2003**, *32*, 577–585.
12. Great Barrier Reef Marine Park Authority. *Water Quality Guidelines for the Great Barrier Reef Marine Park*; Great Barrier Reef Marine Park Authority: Townsville, QLD, Australia, 2009.
13. Brinkman, R.; Wolanski, E.; Deleersnijder, E.; McAllister, F.; Skirving, W. Oceanic inflow from the Coral Sea into the Great Barrier Reef. *Estuar. Coast. Shelf Sci.* **2002**, *54*, 655–668.
14. Choukroun, S.; Ridd, P.V.; Brinkman, R.; McKinna, L.I.W. On the surface circulation in the western Coral Sea and residence times in the Great Barrier Reef. *J. Geophys. Res.* **2010**, doi:10.1029/2009JC005761.
15. Weeks, S.; Bakun, A.; Steinberg, C.; Brinkman, R.; Hoegh-Guldberg, O. The Capricorn Eddy: A prominent driver of the ecology and future of the southern Great Barrier Reef. *Coral Reef.* **2010**, *29*, 975–985.
16. Hancock, G.J.; Webster, I.T.; Stieglitz, T.C. Horizontal mixing of Great Barrier Reef waters: Offshore diffusivity determined from radium isotope distribution. *J. Geophys. Res.-Oceans* **2006**, doi:10.1029/2006JC003608.
17. Wang, Y.; Ridd, P.V.; Heron, M.L.; Stieglitz, T.C.; Orpin, A.R. Flushing time of solutes and pollutants in the central Great Barrier Reef lagoon, Australia. *Mar. Freshwater Res.* **2007**, *58*, 778–791.
18. Luick, J.L.; Mason, L.; Hardy, T.; Furnas, M.J. Circulation in the Great Barrier Reef Lagoon using numerical tracers and *in situ* data. *Cont. Shelf Res.* **2007**, *27*, 757–778.
19. Devlin, M.; Schaffelke, B. Spatial extent of riverine flood plumes and exposure of marine ecosystems in the Tully coastal region, Great Barrier Reef. *Mar. Freshwater Res.* **2009**, *60*, 1109–1122.

20. Schroeder, T.; Devlin, M.J.; Brando, V.E.; Dekker, A.G.; Brodie, J.E.; Clementson, L.A.; McKinna, L. Inter-annual variability of wet season freshwater plume extent into the Great Barrier Reef lagoon based on satellite coastal ocean colour observations. *Mar. Pollut. Bull.* **2012**, *65*, 210–223.
21. Morel, A.; Huot, Y.; Gentili, B.; Werdell, P.J.; Hooker, S.B.; Franz, B.A. Examining the consistency of products derived from various ocean color sensors in open ocean (Case 1) waters in the perspective of a multi-sensor approach. *Remote Sens. Environ.* **2007**, *111*, 69–88.
22. McClain, C.R. A decade of satellite ocean color observations. *Ann. Rev. Mar. Sci.* **2009**, *1*, 19–42.
23. Bailey, S.W.; Werdell, P.J. A multi-sensor approach for the on-orbit validation of ocean color satellite data products. *Remote Sens. Environ.* **2006**, *102*, 12–23.
24. Yoder, J.A.; Schollaert, S.E.; O'Reilly, J.E. Climatological phytoplankton chlorophyll and sea surface temperature patterns in continental shelf and slope waters off the northeast US coast. *Limnol. Oceanogr.* **2002**, *47*, 672–682.
25. Mühlenstädt, T.; Kuhnt, S. Kernel interpolation. *Comput. Stat. Data Anal.* **2011**, *55*, 2962–2974.
26. Andrews, J.C.; Furnas, M.J. Subsurface intrusions of Coral Sea water into the central Great Barrier Reef. Structures and shelf-scale dynamics. *Cont. Shelf Res.* **1986**, *6*, 491–514.
27. Burrage, D.M.; Black, K.P.; Ness, K.F. Long-term current predictions in the central GBR. *Cont. Shelf Res.* **1994**, *14*, 803–829.
28. Ridgway, K.R.; Godfrey, J.S. Seasonal cycle of the East Australian current. *J. Geophys. Res.* **1997**, doi:10.1029/97JC00227.
29. Berkelmans, R.; Weeks, S.J.; Steinberg, C.R. Upwelling linked to warm summers and bleaching on the Great Barrier Reef. *Limnol. Oceanogr.* **2010**, *55*, 2634–2644.
30. Evans, J.L.; Allan, R.J. El-Nino Southern Oscillation modification to the structure of the monsoon and tropical cyclone activity in the Australasian region. *Int. J. Climatol.* **1992**, *12*, 611–623.
31. Lough, J.M. Climate Variability and Change on the Great Barrier Reef. In *Oceanographic Processes of Coral Reefs: Physical and Biological Links in the Great Barrier Reef*; Wolanski, E., Ed.; CRC Press: Bocan Raton, FL, USA, 2001; pp. 269–300.
32. Hung, C.W.; Yanai, M. Factors contributing to the onset of the Australian summer monsoon. *Quar. J. Roy. Meteorol. Soc.* **2004**, *130*, 739–758.
33. Lough, J.M. Climate and Climate Change on the Great Barrier Reef. In *Climate Change and the Great Barrier Reef: A Vulnerability Assessment*; Johnson, J.E., Marshall, P.A., Great Barrier Reef Marine Park Authority, Eds.; Great Barrier Reef Marine Park Authority: Townsville, QLD, Australia, 2007; p. 818.
34. Devlin, M.; Brodie, J.; Wenger, A.; da Silva, E.; Alvarez-Romero, J.G.; Waterhouse, J.; McKenzie, L. Extreme Weather Conditions in the Great Barrier Reef: Drivers of Change? In *Proceedings of the 12th International Coral Reef Symposium*, Cairns, QLD, Australia, 9–13 July 2012.